JOURNAL OF MATERIALS SCIENCE **35** (2000) 813–820

Silver diffusion and microstructure in LTCC multilayer couplers for high frequency applications

KWANG BO SHIM*, NAM TAE CHO*, SEON WOO LEE‡,§
**Ceramic Processing Research Center, and ‡Ceramic Materials Research Institute, Hanyang University, Seoul 133-791, Korea*
E-mail: seonlee@shinbiro.com

Low temperature cofired glass ceramic-Ag metal electrode (LTCC) systems were investigated in relation to Ag diffusion and microstructural development in the fabrication of high frequency couplers. Sintering temperature was in a range of 825 °C–975 °C. Ag diffusion was not observed below 875 °C but densification of the electrode was greatly improved. At higher temperature above 900 °C, Ag ions were diffused through glass phases containing Pb and alkali ions. Crystalline phases behaved as a barrier for the Ag diffusion. With increasing sintering temperature, glass infiltration to the electrode also occurred due to increased fluidity of the glass phase and the electrode line were severely deformed and damaged.

1. Introduction

Recently, wireless telecommunications markets have been explosively multiplied in response to the rapid progress in communication technologies and the growing demand on advanced data transference. On the other side, competitions between the manufacturers of the wireless communication components have been accelerated in parallel to the widening of the marketplaces as in the cases of PCS (personal communication system), GPS (global positioning system), SBS (satellite broadcasting system), Internet etc. Therefore the manufacturers are focusing attention on improving the electronic devices in order to survive under the violent environments. The pressing issues are miniaturization, multi-functionalization, lighter weight, lower cost, and higher efficiency and performance. These demands can be achieved by establishing manufacturing techniques with high predictability and reliability. As a result, low temperature cofired ceramic (LTCC) systems have been adopted as a solution for advanced microelectronic packaging in high frequency applications [1–4]. LTCC processes are relatively simple and have less limitation in forming variable complex shapes or in modulating integrated circuits compared with the conventional processes [5–7].

When conventional dielectric ceramics are used as insulating substrate layers, precious metals, such as Pt or Pd with high melting temperature, must be employed as internal electrodes due to high sintering temperature. The quality factor Q of such a multilayer ceramic device is inversely related to the transmission line power loss of a wave signal [8]. The signal loss mainly relies on the conduction loss of the internal electrode in high frequency ranges, whereas it depends on the dielectric loss of the substrate in low frequency ranges [9, 10]. For high frequency, low loss and hybrid circuit applications, therefore, it is much easier and more effective to use high conductive metals such as Ag or Cu. This fact forces the cofiring substrate system to have a low firing temperature due to the low melting temperatures of such metal electrodes.

In general, the substrate materials of LTCC systems are crystallizable glass systems or a mixture of dielectric fillers (Al_2O_3 or ferroelectrics) and glasses (borosilicate glasses) [5, 11]. The filler is used to improve mechanical strength and insulation of substrates and to prevent warpage due to the surface tension of glass during firing. This LTCC system offers flexibility in control of the dielectric properties of the substrates by manipulating the glass composition or the amount of the filler. In the manufacturing process of the LTCC electronic devices, the firing of the LTCC system is normally accomplished by two stages [12, 13] of binder burnout and sintering.

To give a guarantee for the reliable performance of the LTCC device, the microstructures of the substrate and the metal internal electrode should be carefully controlled. The key factors determining the microstructure are governed by sintering behavior. During the burnout process, the decomposition of organic binders evolves gases and generates pores in the internal electrode as well as in the substrate, thereby resulting in deformation of the metal-substrate interface [14]. There are still some problems in using Ag or Cu metal as the

§ Author to whom all correspondence should be addressed.

internal electrode, which are metal oxidation, diffusion and migration during firing, micro-cracks at the interface or segregation between the substrate and the electrode due to thermal expansion, thermal breakdown caused by thermal shock etc. [15, 16]. In a high frequency range, for example, the roughness and density of the electrode line is the critical factors in determining the electrical properties of the devices due to the skin effect [5, 8, 17, 18]. Metal migration may also cause current leakage and dielectric breakdown [19]. The glass substrate—metal electrode interactions are influenced mainly by the softening or viscous flow of glass phases, which causes the formation of a secondary phase, the deformation of electrode lines or metal electrode migration [20].

Therefore it is of importance to understand the sintering behavior of the glass ceramic—metal system and mechanisms of metal diffusion/migration in order to fabricate reliable LTCC devices and control their properties. In this work, we used commercial glass ceramic thick films and Ag paste to investigate microstructural development and Ag diffusion with firing conditions.

2. Experimental procedures

To fabricate multilayered glass ceramic couplers, the thick film tape was cut off in a given size and a Ag electrode circuit was screen-printed on each sheet. The sheets were stacked and laminated at 70 °C with 21 MPa for 5 min. Based on a DTA (differential thermal analysis) result, the laminated samples were heated to burn out organic binders at 400 °C for 1hr in air and fired in a range of 825 °C–975 °C for a given time with a heating rate of 10 °C/min. XRD (X-ray diffraction), EDXA (electron dispersive X-ray analysis), EPMA (electron-probe microanalysis) and SIMS (secondary ion mass spectroscopy) were carried out for phase identification, microstructural and microchemical analyses, and Ag diffusion analysis. In order to investigate the electrode line thickness and deformation using both optic and electron microscopes, samples were cut in a angle of 45 degrees to the stacked direction of the substrate layers. The mean thickness of the electrode line was obtained by measuring the line thickness at more than 150 points.

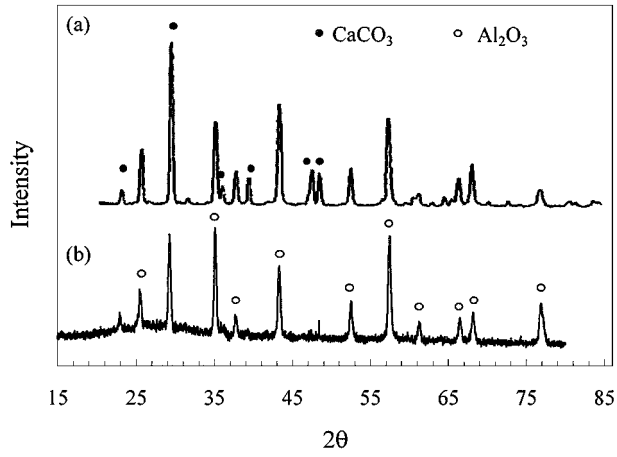

Figure 1 XRD patterns of (a) $CaCO_3$+ Al_2O_3 standard sample and (b) the glass ceramic green sheet.

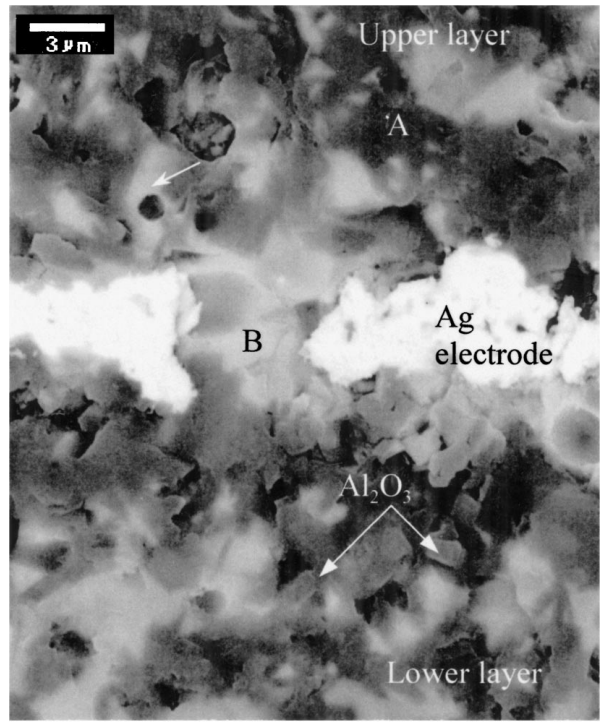

Figure 2 Microstructure and EDX analysis for the substrate-silver interface in the LTCC coupler sintered at 825 °C for 20 min: (a) SEM backscattered image and (b) EDXA spectra.

3. Results and discussion

Chemical analyses using SIMS, EPMA and XRD suggested that the commercial green sheet used in this study be composed of alumina, calcite and a lead borosilicate glass containing Li, Na, K, Mg as modifiers or impurities. Alumina and calcite powders were used as fillers in view of the XRD patterns of Fig. 1 for the green sheet and a $CaCO_3/Al_2O_3$ standard sample. A typical BS (backscattered) SEM image of Fig. 2 for the sintered sample showed two phases with different contrast in the substrate region. The one is a dark area marked as A, which was identified as alumina particles or an Al-Si-Ca phase from EDX analysis. The XRD patterns in Fig. 3 show that an anorthite peak appears as a new crystalline phase instead of the diminution of the calcite peak with increasing sintering temperature, indicating that the Al-Si-Ca phase is anorthite. The other is a bright area marked as B, which is a Si-Al-Pb glass phase. This glass phase built a layer along the electrode surface or around pores due to glass migration following a softening of glass phases. The glass migration brings about formation of a bonding zone between the electrode metal and dielectric substrate or between the electrode metal particles, and thus improves reciprocal adherence between them [21–23]. However, the glass layer plays a role of resistors, leading deterioration in electrical performance.

The typical semi-quantitative data obtained by EDX-ZAF correction for the Al-Si-Ca and glassy phases were given in Table I. Light elements such as lithium and boron were not listed in this table because of detection difficulties, which are normally experienced in the microchemical analysis due to absorption effects by

TABLE I EDX-ZAF analysis for typical crystalline and glass phases in the glass ceramic substrate after firing

Elements	Crystalline phase	Glassy phase
	Atomic %	
O	61.19	61.35
Al	25.29	10.99
Si	13.27	20.42
Na	0.90	1.24
K	0	1.27
Ca	1.98	1.57
Pb	0.31	2.56

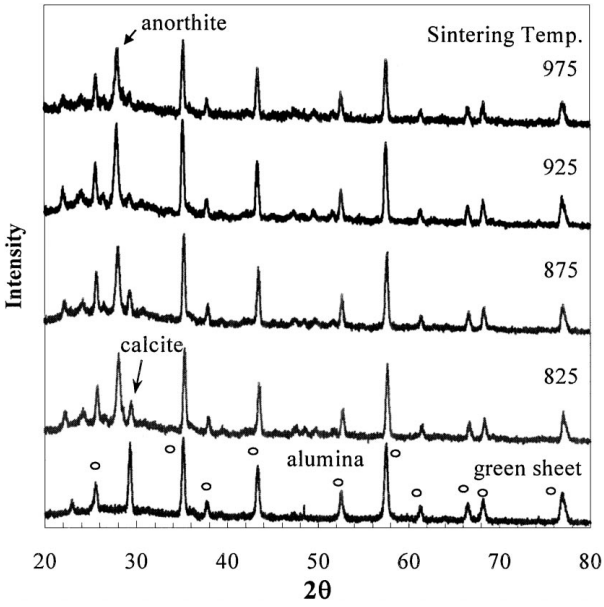

Figure 3 XRD patterns of glass ceramic substrates with sintering temperature.

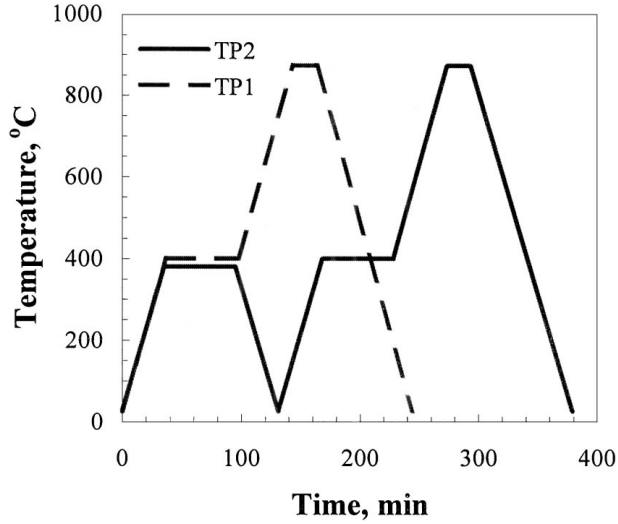

Figure 4 Heating profiles for binder burnout.

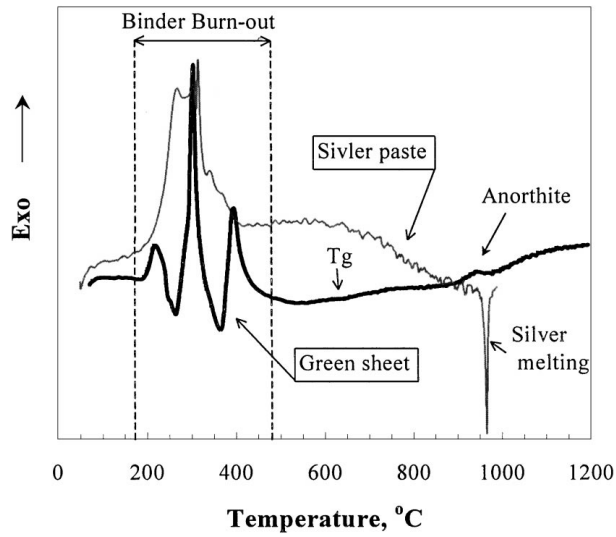

Figure 5 DTA plots of the green sheet and Ag paste (Heating rate:10 °C/min in air).

protection windows. Table I shows that the atomic ratios of Al to Si are about 2 : 1 in the dark area of the Al-Si-Ca crystalline phase and about 1 : 2 in the bright area of the glassy phase. It is of interest to note that the concentrations of Ca ions in the crystalline phase and of Pb ions in the glassy phase are much higher compared with those of other modifiers. Furthermore, the modifiers are rare in the crystalline phase but exist in an equal concentration in the glassy phase. This compositional difference is expected to influence Ag diffusion and microstructural development at the Ag electrode—substrate interface.

In order to investigate the effect of binder burnout, the multilayered green bodies were fired with heating conditions marked as TP1 (two-stage) and TP2 (three-stage) as depicted in Fig. 4 which were based on the DTA results of Fig. 5. The TP1 heating schedule was comprised of one-stage binder burnout at 400 °C and sintering at 875 °C. TP2 was given by a two-stage burnout process to enhance the organic decomposition. The DTA curve of Fig. 5 showed that three kinds of organic additives contained in the green sheet were decomposed between 180 °C and 450. The glass transition temperature was about 640 °C and the exothermic peak appearing at 930 °C was attributed to the formation of anorthite. The Ag paste used also contained more than two kinds of organic additives and their decomposition temperature was in a similar range as that for the green sheet. After firing the multilayered green bodies, the mean thickness of the Ag electrode line changed from 16 μm in the dried green body to 6.56 μm $\pm$ 2 μm in the TP1 sample and 6.23 μm $\pm$ 2 μm in the TP2 sample respectively. The Ag electrode was more densified in the TP2 sample than the TP1 sample due to the moderate and longer heating schedule.

The SEM images of Fig. 6 exhibited substantial pores created in both of the substrate and electrode regions during the decomposition process. Compared with the TP2 sample, the TP1 sample showed larger pore size and higher pore density. As seen in Fig. 6a, a rapid evolution of gases generated by the decomposition of the organic binders introduced an abnormally large spot in the middle of the electrode region. Entrapped gases can be also another source setting up this kind of the anomalous pore at higher temperature than the decomposition temperature. If the decomposition process is not enough to remove organic binders like TP1, therefore,

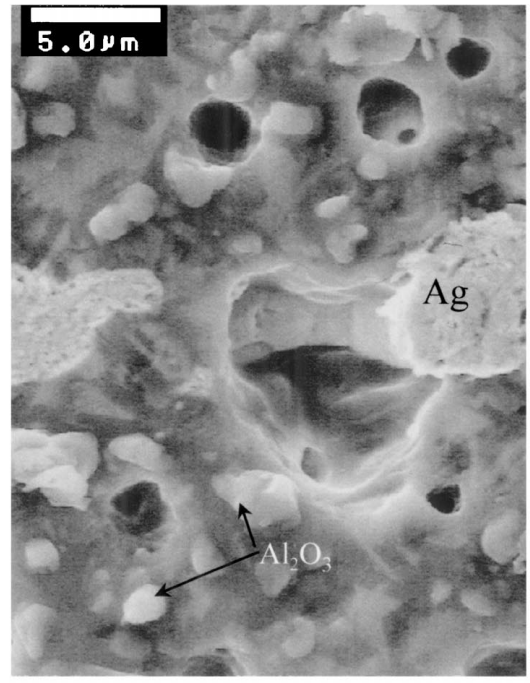

(a)

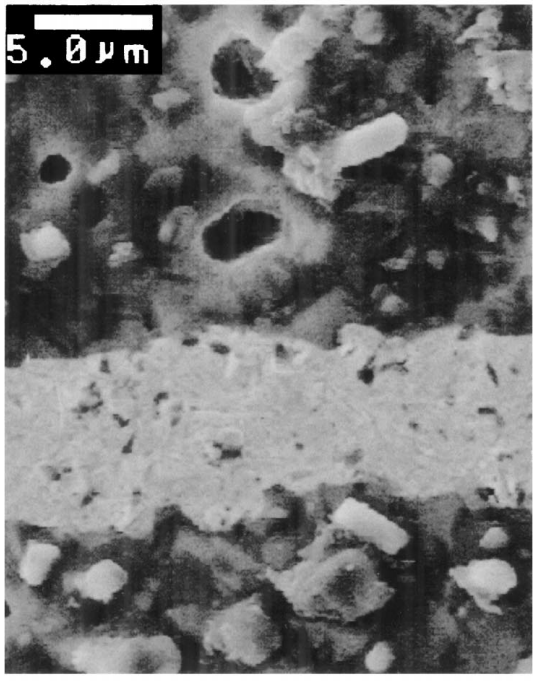

(b)

Figure 6 Microstructures of the glass ceramic substrate and the silver electrode in LTCC (a) TP1 and (b) TP2 samples.

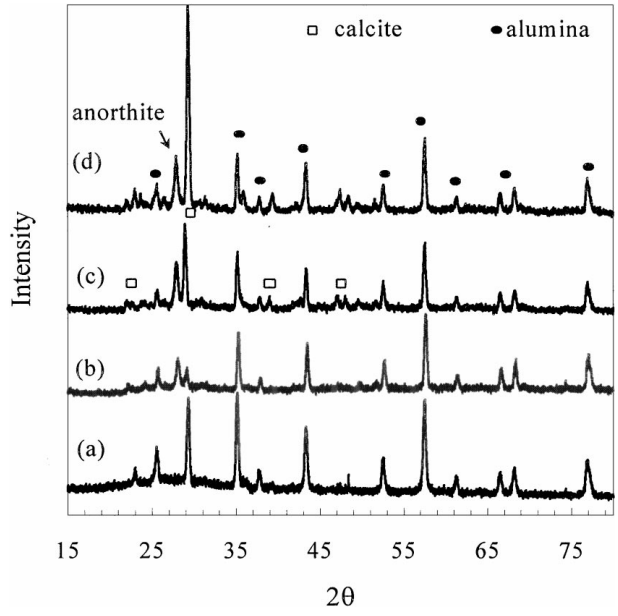

Figure 7 XRD patterns of TP1 sample sintered at 875 °C: (a) green sheet, (b) 20 min, (c) 40 min, (d) 60 min, (e) 120 min and (f) 240 min.

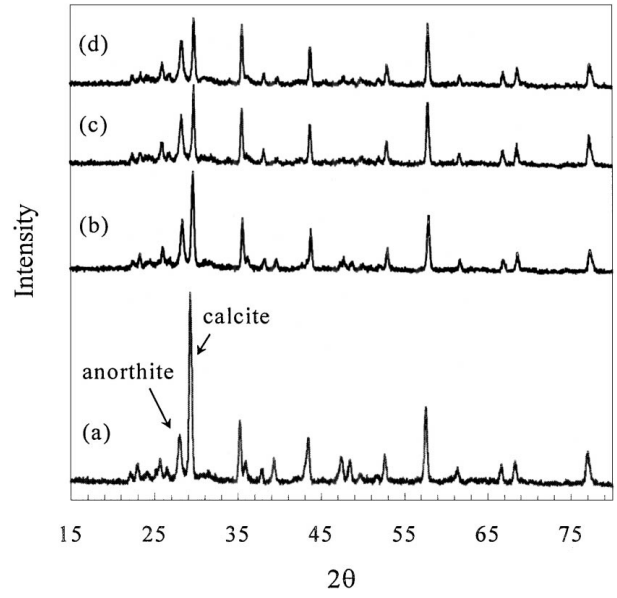

Figure 8 XRD patterns of TP2 sample sintered at 875 °C: (a) green sheet, (b) 20 min, (c) 40 min, (d) 60 min, (e) 120 min and (f) 240 min.

the binder residues or trapped gasses in the glass or electrode matrix can provoke a burst of the gas out of the glass phase that is softened at higher temperature [24]. The abnormal pore allowed the interruption of the electrode line and the infiltration of the substrate materials into the pore as shown in Fig. 6a. Thus it is necessary to control precisely the binder decomposition process.

The XRD patterns of the TP1 and TP2 samples with varying sintering time revealed interesting results as shown in Figs 7, 8. Alumina and anorthite peaks in the both samples were not much changed with varying sintering time, which indicates that the formation of anorthite is instantly terminated at an initial stage of sintering, regardless of decomposition conditions or firing schedules. There are also converse trends in the XRD peaks of calcite. The calcite peak intensity in the TP1 sample increased with increasing sintering time in contrast with the decrease in the TP2 sample. An insufficient decomposition process could induce entrapped gases or organic residues in the substrate as mentioned above. These may produce favorable conditions for the formation of calcite as becoming a source providing CO_2 gas and increasing the partial pressure of the CO_2 gas. SEM observations showed that unknown phases, considered to be $CaCO_3$, were formed around the pores predominantly.

Ag diffusion might be a primary problem in its use because of its detrimental effects on the electrical performance and microstructure of multilayer LTCC

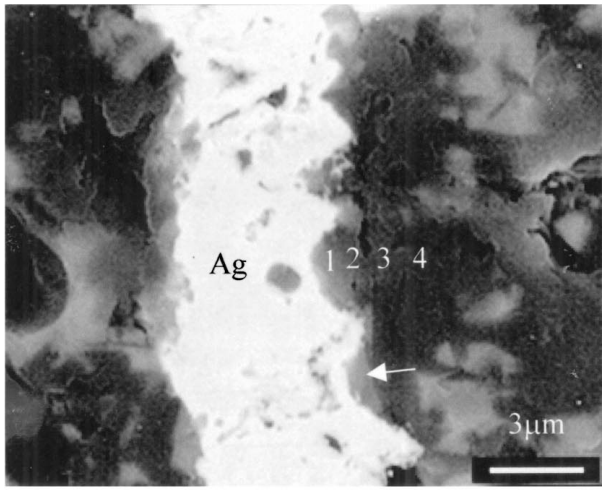

(a)

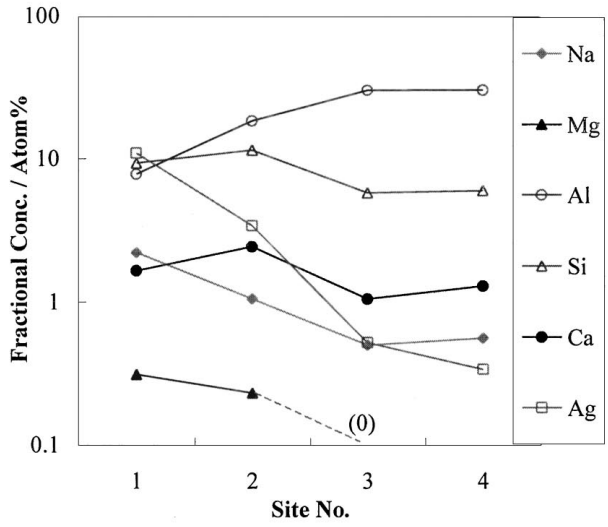

(b)

Figure 9 EDX ZAF point analysis for the crystalline phase of TP1 sample: (a) SEM BS image and (b) quantitative analysis result of the sites marked in (a).

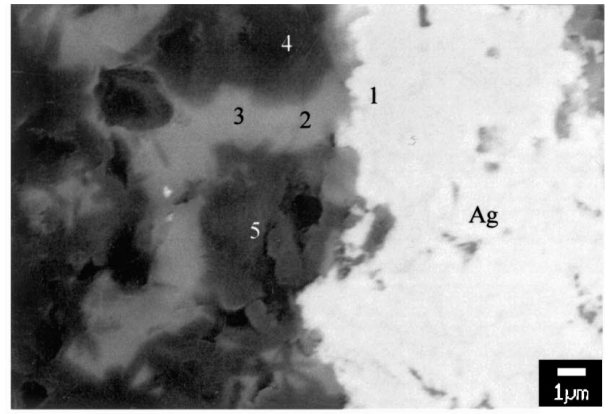

(a)

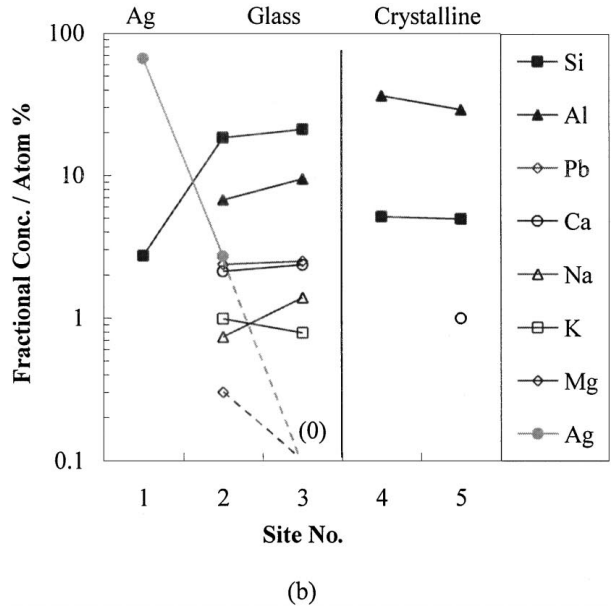

(b)

Figure 10 EDX ZAF point analysis for the glass phase of TP1 sample: (a) SEM BS image and (b) quantitative analysis result of the sites marked in (a).

devices [15, 16]. Glass migration is also closely interrelated to the Ag diffusion and the microstructures of the substrate and electrode [25]. Figs 9, 10 show the polished surfaces of the TP1 sample and their EDXA-ZAF correction results. The EDX point analysis was conducted at the sites marked as the numerical numbers along the crystalline and glass phases respectively.

As seen in Fig. 9a, the Ag electrode surface line was severely deformed and an interface layer marked as a white arrow was formed along the electrode. The compositional changes in Fig. 9b with the distance from the Ag/substrate interface (site 1 → 4) showed a tendency of passing from a glass phase to a crystalline phase. As the distance increased, the Al concentration increased in opposite to the trend of a decrease in the Si concentration. The concentrations of modifiers such as Na, K were insignificant and showed a trend of decreasing with increasing distance, but the Ca concentration was not altered. Pb ions were not detected or can be negligible in this region (sites 1–4), even though the substrate contained a large amount of the Pb ions. This fact confirmed that the glass phase forming the interface layer did not originate from the substrate but from the electrode region. A significant amount of Ag ions was also observed along the interface and its concentration rapidly decreased with standing off from the Ag electrode. The region where the interface layer of the glass phase was formed was the place that was occupied by the Ag electrode. These facts also pointed out that the Ag ions moved toward the inside of the Ag electrode instead of diffusing into the substrate. The crystalline phases marked as 3 and 4 in Fig. 9a may form a block against the Ag diffusion. Consequently, it can be assumed that the glass region is formed by the glass migration from the electrode center to the interface and by the Ag diffusion from the interface to the electrode center. In addition, the fact that the amount of Ag ions was negligible in the crystalline phase of the sites 3 and 4 demonstrates that the Ag diffusion took place through a medium of the glass phase, not the crystalline phase. These results can be also confirmed from Fig. 10, where the Ag ions were diffused along only the glass phase line numbered from 1 to 3 and the modifiers except Ca ions were not detected in the crystalline phases numbered as 4 and 5.

TABLE II Ag concentrations with the distance from the Ag/substrate interface, measured by EPMA

Phase		Glass			Crystalline		
Sintering temp. (°C)		Concentration (element %)					
Distance (μm)		875	925	975	875	925	975
Electrode	*−4	—	—	60.65	—	—	—
region, (D_{Ag})	−2	96.20	93.89	78.61			77.86
Interface	0	96.00	93.00	67.63	95.54		76.26
Substrate	2	1.06	6.91	4.36	0.55	0.88	27.34
region, (D_{sub})	4	0.68	5.51	0.31	0.43	0.09	—
	6	0.66	0.26	0.34	—	—	—
	8	—	0.24	—	—	—	—

(*Negative sign indicates that the analyzed point is in the electrode region.)

To investigate the diffusion behavior of Ag ions with sintering temperature, EPMA was performed on the multilayer LTCC coupler samples that were sintered between 825 °C–975 °C. The spot size of the electron beam was 2 μm. Table II represented Ag concentrations in the substrate and electrode regions with the distance from the Ag electrode/substrate interface. The distance from the Ag/substrate interface was designated as D_{Ag} and D_{Sub} for the substrate and electrode regions, respectively. As mentioned previously, the above Ag diffusion was observed only in the glass phase. From the quantitative data for the glass phase in Table II, it turned out that the Ag diffusion was dependent on the sintering temperature. For the sample sintered at 875 °C, the Ag concentration was 98 elmt% at the interface of Ag/substrate ($D = 0$) but decreased with increasing D, that is, about 1 elmt% at $D_{sub} = 4$ μm and 0.66–0.68 elmt% at $D_{sub} = 2$–4 μm.

In a microanalysis using either EDX or EPMA, there are some points which must be taken into account in interpreting the quantitative data obtained from bulk specimens. These are absorption or emission of X-ray radiation. The most important practical point is the electron scattering with the specimen. The combined effects of spreading and penetration lead to X-ray radiation being generated in a volume within the specimen whose effective size is much greater than might be anticipated from the diameter of the original electron probe. The actual size of the emitting volume varies with beam energy and the atomic number of elements. This fact may produce wrong information on the site analyzed [26]. Therefore it is assumed that the possibility of detecting Ag ions, which does not originate from the diffused Ag but from the Ag electrode, will be raised as D approaches the electrode. Thus at 875 °C, the small amount of the Ag ions detected at $D_{sub} = 2$–4 μm is considered to arise from the Ag electrode due to the electron scattering effect rather than the Ag diffusion. In the samples sintered at 925 °C and 975 °C, however, the Ag concentration reaches about 4.4–6.9 elmt% at $D_{sub} = 2$–4 μm, which was attributed to the Ag ions diffused through the glass phase. The Ag diffusion did not take place in the crystalline region by showing less than 1 elmt% of Ag ions at $D_{sub} = 2$–4 μm below 925 °C. However, a very large Ag concentration of 25 elmt% at $D_{sub} = 2$ μm was observed at 975 °C due to silver melting as shown in Fig. 11d.

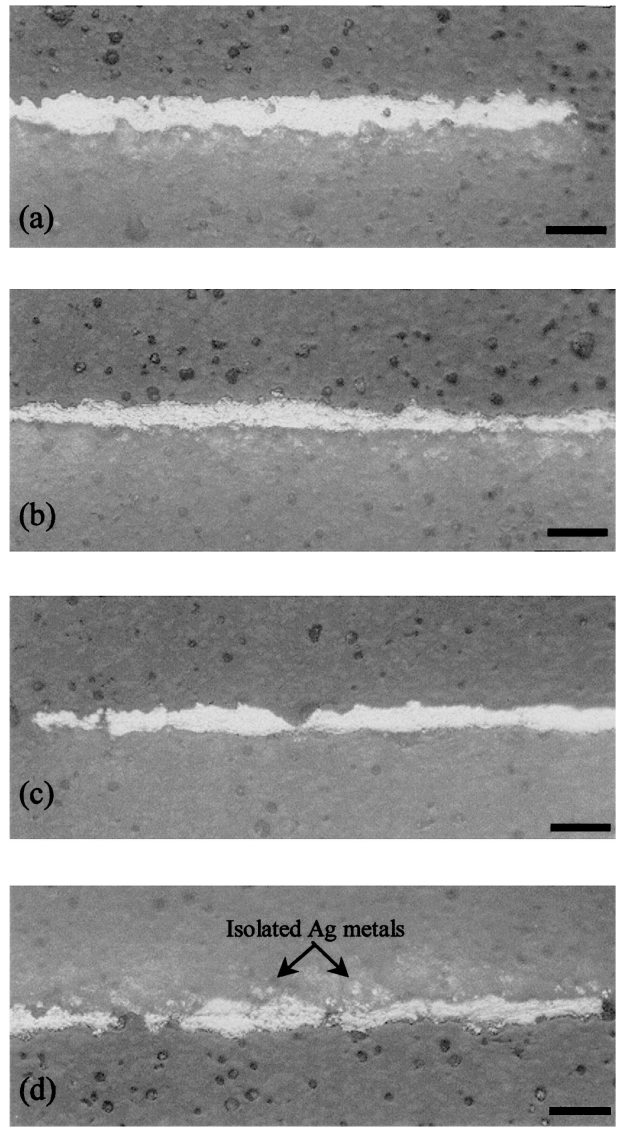

Figure 11 Optical images of Ag electrode lines sintered at (a) 825 °C, (b) 875 °C, (c) 925 °C and (d) 975 °C.

Fig. 12 shows compositional changes in the glass and crystalline with varying sintering temperature. For the glass phase of Fig. 12a, the peak intensities of Al and Si were not much changed. Meanwhile, the Pb peak intensity decreased with increasing sintering temperature compared with the trivial changes in those of K and Ca ions. The loss of Pb ions is assumed to be due

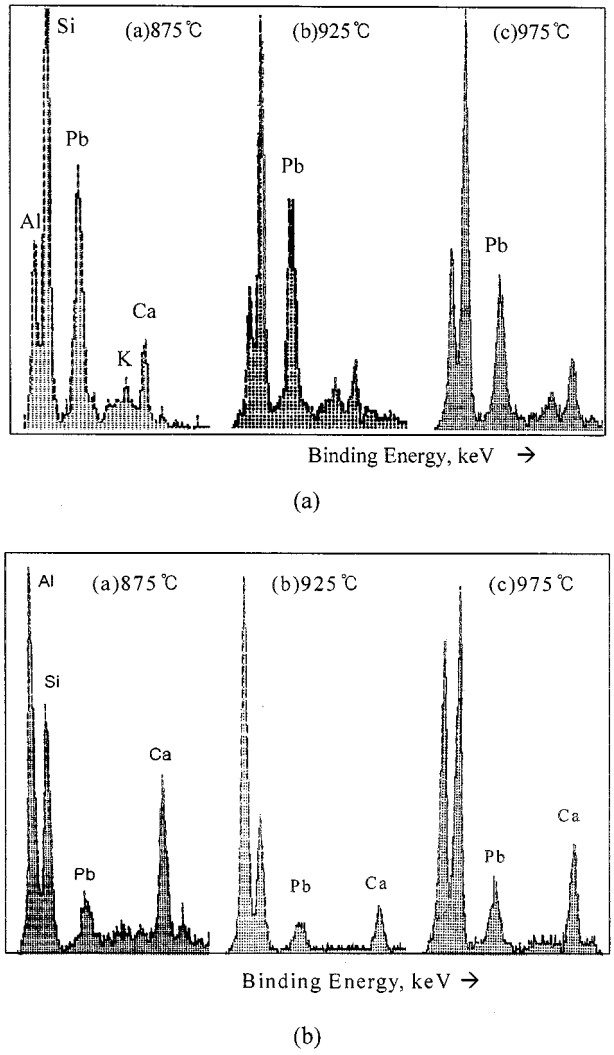

Figure 12 The compositional change in the EDX spectra of (a) the glass phases and (b) the crystalline phases with sintering temperature.

to Pb diffusion or vaporization. In the crystalline phase, the Si peak became stronger with increasing sintering temperature at the expense of a decrease in the Al peak intensity. The ratio of Pb to Ca ions also increased with increasing sintering temperature (Fig. 12b). These facts may reflect the transformation of Al_2O_3 crystalline particles into a glass phase due to high sintering temperature, which may produce a favorable circumstance for Ag diffusion.

Such an observation can introduce the following conclusion: the crystallization of glass phases at the boundaries of alumina particles, which act as nuclei, stands for a phase separation of changing the residual glass phase to contain more modifiers such as Na, K, Mg. At low sintering temperature, Ag ions diffuse through this glass phase with open structure. With increasing sintering temperature, however, alumina particles begin to dissolve into the glass phase due to a decrease of the glass viscosity, giving rise to an exciting diffusion of Pb and Ag ions. The Ag concentrations in the electrode region, which is close to the glass phase, decreased with increasing sintering temperature as 96 elmt% at 875 °C, 93 elmt% at 925 °C and 78 elmt% at 975 °C. Furthermore, when sintered at 975 °C, the Ag concentration showed a decreasing gradient in the direction

TABLE III Variation of electrode line thickness with sintering temperature

Sintering temperature (°C)	Electrode line thickness (μm)
825	5.85 ± 1.43
850	4.67 ± 0.86
875	4.49 ± 1.48
900	4.86 ± 1.34
925	5.37 ± 1.21
950	5.79 ± 1.46
975	4.85 ± 1.48

of the electrode/substrate interface from the electrode center. These facts support the glass migration into the electrode as well as the Ag diffusion into the substrate.

The deformation of the electrode line was carefully examined in relation to the viscous behaviors of the substrate and electrode. At a low sintering temperature of 825 °C, the electrode crests with acute angles were observed on the substrate (Fig. 11a). The convex of the crest normally directed to the substrate. SEM observations showed that the Ag electrode exhibited poor sinterability and large porosity when sintered at 825 °C. It was reported [22] that interfacial reactions change surface tension and affect Ag/substrate wetting, where Ag oxide (Ag_2O) formed at the interfaces has a key role. A trend forming the convex may come from the high surface tension of the Ag metal and a viscous flow of the glass phase showing a good adherence. With further increase of the sintering temperature, the electrode surface became smooth (Fig. 11b) due to a liquidus sintering of Ag metals. Above 925 °C, the electrode line was collapsed and severely indented due to the energetic Ag diffusion and glass migration (Fig. 11c) or even disappeared over a long distance at 975 °C which is higher than the Ag melting temperature (Fig. 11d).

The liquid sintering of Ag metals was activated by the increase of the sintering temperature, which resulted in a leveling of the electrode line and densification by removing micropores from the electrode. The densification can be also led by the glass migration as exhibited in Fig. 4a. The variation of the electrode line thickness in Table III indicates that the densification is maximized at 875 °C. The increase of sintering temperature above 900 °C lowers the viscosity of the glass phase leading glass infiltration to the electrode region and activates Ag diffusion, as shown in Table II and Fig. 12. Thus, the line thickness re-increased above 875 °C and showed a maximum at 950 °C. However, the line thickness again decreased at 975 °C, because the electrode is extremely damaged due to melting.

4. Conclusions

Ag diffusion and interfacial behaviors in the LTCC system were investigated with sintering conditions.

1) Pore size and porosity were largely dependent on the binder burnout process. A rapid evolution of gases due to organic binder burnout makes a detrimental deformation in the electrode. Remaining binders or gases

trapped in the substrates bring about the formation of $CaCO_3$ around pores. Thus a moderate decomposition process is necessary.

2) Ag diffusion takes place only through glass phases containing Pb and modifiers. Crystalline phase of Al_2O_3 and anorthite form barriers against the Ag diffusion. At low sintering temperature below 875 °C, the Ag ions were not diffused and densification of the electrode was dominated. Above 900 °C, however, Ag diffusion through the glass substrate and glass penetration into the electrode actively occurred, which caused a severe deformation of the electrode line.

Acknowledgement

The authors would like to thank KRF (Korea Research Foundation) for supporting this work.

References

1. C. MAKIHARA, K. IKEDA, H. WADA, Y. SAWA and S. TANAHASHI, in ISHM 1994 Proceedings, p. 243.
2. JAE Y. PARK and M. G. ALLEN, in ISHM 1996 Proceedings, p. 120.
3. W. MARSH, M. KLINE, F. KUSS and D. STRACK, in ISHM 1996 Proceedings, p. 230.
4. H. MANDAI, N. NAKAJIMA and K. TONGEGAWA, in IMC 1996 Proceedings, p. 183.
5. A. J. PILOTO, D. P. PARTLOW and K. ZAHI, in "Ceramics: Charting the Future," Vol. 3D, edited by P. Vincenzini (Faenza, Techna, 1995) p. 2465.
6. R. R. TUMMALA, *J. Amer. Ceram. Soc.* **74**(5) (1991) 895.
7. M. F. BENDER, F. K. PATTERSON, E. A. KEMP and J. E. GANTZHORN, JR., in ISHM 1988 Proceedings, p. 12.
8. A. J. MOULSON and J. M. HERBERT, "Electroceramics: Chap. 5 Dielectrics and Insulators" (Chapman & Hall, London, 1990).
9. H. KAGATA, *et al.*, *National Technical Report* **4**(1) (1994) 17.
10. J. R. TYLER and D. J. GASPER, in ISHM 1989 Proceedings, p. 390.
11. K. KONDO, M. OKUYMAM and Y. SHIBATA, in "Advanced in Ceramics," Vol.19, edited by J. B. Blum and W. R. Cannon (Am. Ceram. Soc., Westerville, OH, 1986) p. 77.
12. W. S. HACKENBERGER, T. R. SHROUT, J. P. DOUGHERTY and R. F. SPEYER, in ISHM 1992 Proceedings, p. 82.
13. W. S. HACKENBERGER, T. R. SHROUT and J. P. DOUGHERTY, in ISHM 1993 Proceedings, p. 215.
14. J. G. PEPIN, W. BORLAND, P. O'CALLAGHAN and R. J. S. YOUNG, *J. Am. Ceram. Soc.* **72**(12) (1989) 2287.
15. D. J. GASPER, F. K. PATTERSON and B. L. IORFIDO, in ISHM 1988 Proceedings, p. 246.
16. J. B. DIXON, D. T. ROONEY and N. T. CASTELLO, in ISHM 1976 Proceedings, p. 267.
17. F. UCHIKOBA, S. NAKAJIMA and T. ITO, *J. Ceram. Soc. Japan* **103**(9) (1995) 969.
18. S. VASUDEVAN, in ISHM 1996 Proceedings, p. 40.
19. TOM MARTIN and DON SCHROEDER, in ISHM 1994 Proceedings, p. 295.
20. T. YAMAGUCHI, in IMC 1996 Proceedings, Omiya, April, p. 245.
21. V. K. NAGESH, A. P. TOMSIA and J. A. PASK, *J. Mater. Sci.* **18** (1983) 2173.
22. V. F. ZACKAY, D. W. MITCHELL, S. P. MITOFF and J. A. PASK, *J. Amer. Ceram. Soc.* **36**(3) (1953) 84.
23. A. K. VARSHNEYA and S. C. CHERUKURI, in "Ceramic Transactions: Glasses for Electronic Applications," Vol. 20, edited by K. M. Nair (American Ceramic Society, 1991) p. 387.
24. D. WHITMAN, in International Microelectronics Symposium Proceedings, 1998, p. 421.
25. R. C. SUTTERLIN, G. O. DAYTON and J. V. BIGGERS, *IEEE Trans. on Components, Packaging, and Manufacturing Technology-Part B* **18**(2) (1995) 346.
26. J. I. GOLDSTEIN, A. D. ROMIG, JR., D. E. NEWBURY *et al.*, "Scanning Electron Microscopy and X-ray Microanalysis: Chap. 3 Electron-Specimen Interaction" (Plenum Press, New York, 1992).

Received 16 March
and accepted 17 August 1999